

Upconverting Nanoparticles in Aqueous Media: Not a Dead-End Road. Avoiding Degradation by Using Hydrophobic Polymer Shells

Diego Mendez-Gonzalez,* Vivian Torres Vera, Irene Zabala Gutierrez, Christoph Gerke, Concepción Cascales, Jorge Rubio-Retama, Oscar G. Calderón, Sonia Melle,* and Marco Laurenti*

The stunning optical properties of upconverting nanoparticles (UCNPs) have inspired promising biomedical technologies. Nevertheless, their transfer to aqueous media is often accompanied by intense luminescence quenching, partial dissolution by water, and even complete degradation by molecules such as phosphates. Currently, these are major issues hampering the translation of UCNPs to the clinic. In this work, a strategy is developed to coat and protect β -NaYF₄ UCNPs against these effects, by growing a hydrophobic polymer shell (HPS) through miniemulsion polymerization of styrene (St), or St and methyl methacrylate mixtures. This allows one to obtain single core@shell UCNPs@HPS with a final diameter of \approx 60–70 nm. Stability studies reveal that these HPSs serve as a very effective barrier, impeding polar molecules to affect UCNPs optical properties. Even more, it allows UCNPs to withstand aggressive conditions such as high dilutions (5 μ g mL⁻¹), high phosphate concentrations (100 mM), and high temperatures (70 °C). The physicochemical characterizations prove the potential of HPSs to overcome the current limitations of UCNPs. This strategy, which can be applied to other nanomaterials with similar limitations, paves the way toward more stable and reliable UCNPs with applications in life sciences.

sequential absorption of two or more low energy photons (e.g., Near Infrared) and the subsequent emission of a fewer number of higher energy photons (e.g., visible), photon upconversion is typically accompanied by large anti-Stokes shifts that prevent their luminescence from being contaminated by autofluorescence from surrounding biomolecules. As a result, background-free emissions are obtained. In combination with the absence of blinking, photobleaching, and their long-lived emissions, these properties make UCNPs ideal luminescent probes for applications within biological media.^[2] Lanthanide-doped UCNPs based on fluoride matrices (e.g., β -NaYF₄ and β -NaGdF₄) are currently the most widely used nanomaterials sustaining photon upconversion processes between lanthanides such as Yb³⁺ and Er³⁺, as these matrices allow the best quantum efficiencies due to their inherent low phonon energies.^[3–5] Nevertheless, most of these


UCNPs must be transferred to aqueous media (e.g., biological fluids and buffers) to be effectively used as luminescent probes in bio-applications such as sensing, imaging, and in vitro or in vivo nanothermometry, or as light converters to trigger local photochemical reactions in biological environments.^[6–11]

1. Introduction

Lanthanide-doped upconverting nanoparticles (UCNPs) probably feature one of the most distinctive and stable emissions among photoluminescent materials.^[1] Arising from the

D. Mendez-Gonzalez, V. Torres Vera, I. Zabala Gutierrez, C. Gerke, J. Rubio-Retama, M. Laurenti
Department of Chemistry in Pharmaceutical Sciences
Faculty of Pharmacy Complutense University of Madrid
Plaza Ramon y Cajal 2, Madrid 28040, Spain
E-mail: diegomen@ucm.es; marclaur@ucm.es

D. Mendez-Gonzalez
Nanomaterials for Bioimaging Group (nanoBIG)
Departamento de Física de Materiales
Facultad de Ciencias
Universidad Autónoma de Madrid
C/Francisco Tomás y Valiente 7, Madrid 28049, Spain

 The ORCID identification number(s) for the author(s) of this article can be found under <https://doi.org/10.1002/smll.202105652>.

D. Mendez-Gonzalez, C. Gerke, J. Rubio-Retama, M. Laurenti
Nanobiology Group
Instituto Ramón y Cajal de Investigación
Sanitaria Hospital Ramón y Cajal
Ctra. De Colmenar Viejo, Km. 9100, Madrid 28034, Spain

C. Cascales
Instituto de Ciencia de Materiales de Madrid
Consejo Superior de Investigaciones Científicas CSIC
c/Sor Juana Inés de la Cruz 3, Madrid 28049, Spain
O. G. Calderón, S. Melle
Department of Optics
Faculty of Optics and Optometry Complutense University of Madrid
Avda. Arcos de Jalón 118, Madrid E-28037, Spain
E-mail: smelle@fis.ucm.es

DOI: 10.1002/smll.202105652

Unfortunately, this transfer step to water is highly detrimental to their luminescent properties, and for their bio-applications due to several reasons.^[6–8,12] First, the aqueous transfer of UCNP is normally accompanied by an intense reduction of the lifetime and luminescence of their constituent lanthanides.^[13,14] This is in part due to a surface quenching that stems from the vibrational modes of the hydrophilic molecules used to turn UCNP water-dispersible, but mostly due to a combination of the strong nonradiative relaxation of Yb³⁺ when coupled with water vibrational modes, and the relatively high absorption by water of the wavelength used to excite Yb³⁺-sensitized UCNP (λ_{exc} = 976 nm).^[13,14] Second, the solubility product of UCNP matrices like β-NaYF₄, one of the most efficient and commonly used hosts, is quite low (1.6 × 10⁻²⁶).^[15] However, the high specific surface area of UCNP (≈46.4 m² g⁻¹ for UCNP of Ø = 30 nm), together with the low concentrations normally required in bio-applications, are in such ranges that UCNP often suffer time-dependent structural degradation due to dissolution–reprecipitation of their host matrices in aqueous media.^[16,17] In fact, this effect over the UCNP structural integrity has been reported for concentrations lower than 50 µg mL⁻¹ in nanoparticles with diameters of 25–31 nm.^[15] In this regard, it is reasonable to think that this phenomenon will have an even more deleterious effect in the new generations of UCNP, given the current trend of synthesizing ultrasmall UCNP for biological applications, or designing core/shell UCNP, where the dissolution of the shells used to improve or change their optical properties will result in an important reduction of their luminescence and a change in their optical features.^[18–22] On top of that, increasing the temperature of the medium shifts the solubility equilibrium toward the dissolution of UCNP. Because of this, the application of UCNP in fields such as nanothermometry or platforms that require thermal cycles such as polymerase chain reaction (PCR) is currently very hampered when low concentrations of UCNP are required. Third, the fact that fluoride (F⁻) and lanthanide ions (Ln³⁺) are released to the aqueous medium until reaching the solubility equilibrium has important implications. On the one hand, the presence of chemical species (e.g., phosphates) that can capture free Ln³⁺ and form more stable compounds will displace the solubility equilibrium of the host matrices until the complete dissolution of UCNP occurs.^[23,24] On the other hand, the presence of F⁻ and Ln³⁺ ions in solution raise some questions and concerns about the biocompatibility and bioaccumulation of these ions when using UCNP in biological fluids. As an example, several toxicity issues have already been ascribed to F⁻ and Ln³⁺.^[25–30] Besides, the high phosphate content at specific locations within the body, such as the bones' mineral matrix, may be prone to bioaccumulate Ln³⁺.^[29,31]

These drawbacks urge to develop a strategy that satisfactorily solves these limitations, giving a step forward to ensure realistic prospects for these promising materials in life sciences, while expanding their range of current possible applications. In this direction, different approaches have been explored to alleviate some of these problems. For example, Lahtinen et al. took advantage of the so-called common ion effect (adding KF to aqueous solutions) to hamper dissolution of UCNP when used at low concentrations and room temperature (RT).^[15] In a later work, Palo et al. developed a strategy based on the coating of UCNP with oppositely charged polyelectrolyte bilayers to delay

the disintegration of UCNP, especially during the first 5 h.^[32] A similar layer by layer strategy was used later to help alleviating the quenching exerted by water molecules.^[33] In other works, ligand exchange of UCNP's capping agent by a proper molecule has also proven, in some cases, to hamper this luminescence quenching.^[34] Interestingly, when some phosphate/phosphonate-containing molecules are used in this kind of ligand exchange strategies, the resulting UCNP seem to show enhanced resistance to chemically harmful molecules such as phosphate buffer and acidic media.^[30,33,35] This is explained by the high binding affinity between phosphonate moieties and the Ln³⁺ located at the surface of UCNP, which hampers the release of ions from the host matrix and partially shields against other ligands and water molecules. Nevertheless, not all phosphonates passivate UCNP's surface effectively.^[36] In fact, literature seems to indicate that passivation is often increased by capping agents that simultaneously combine one or more phosphonate/phosphonic groups in one side, which strongly coordinates to the UCNP's surface, and a less polar moiety (e.g., aliphatic chains) on the other side to provide shielding from water and other ligands.^[30,37–39] Interestingly, using capping agents that contain carboxylic or sulfonate groups instead of phosphonate moieties, or just preserving the UCNP's original capping agents (e.g., oleic acid), seem viable strategies to partially protect UCNP from the surrounding aqueous environment as long as these are coated with amphiphatic molecules with long aliphatic chains or polymer chains with reduced polarity.^[39–42] This highlights the importance of creating a relatively robust and effective shielding layer surrounding the UCNP, as this seems to partially limit the diffusion of water and other possible ligands that are capable to exert detrimental effects on the optical properties and structural integrity of UCNP. In fact, the use of an intermediate shielding layer with hydrophobic properties may be one of the best possible approaches, as it would not only contribute to keeping away polar and harmful molecules from diffusing toward the surface of UCNP, but it should partially maintain a local environment resembling the original postsynthetic hydrophobic conditions (e.g., chloroform or hexane dispersions) where UCNP exhibit their best performances. Bearing all this in mind, we present a simple and rationale design of the UCNP's surface that ensures their protection in aqueous media under different harsh conditions. Our approach is based on the combination of two synergic strategies: first, the oleic acid ligands at the surface of UCNP are replaced in nonpolar solvents by 10-methacryloyldecylphosphate (MDP), to achieve surface passivation, colloidal stability in organic media, and a terminal polymerizable group. Second, the dispersion and free-radical miniemulsion polymerization of these UCNP in styrene (St), or a mixture of St and methyl methacrylate (MMA), pursues the formation of a robust hydrophobic shell of controlled thickness that insulates and protects UCNP from aqueous environment. This method is also expected to provide them with colloidal stability in aqueous media due to the presence of polar groups incorporated during the polymerization process. Full optical, morphological, and chemical characterization of the resulting polymer-coated UCNP was carried out, and their resistance to different harsh conditions such as phosphate buffer, very high dilutions, and high temperatures was studied. A stunning improvement

in UCNPs' chemical resistance is proved, suggesting that this kind of strategy may pave the way toward safer UCNPs with more reliable optical properties and expanded applications in life sciences.

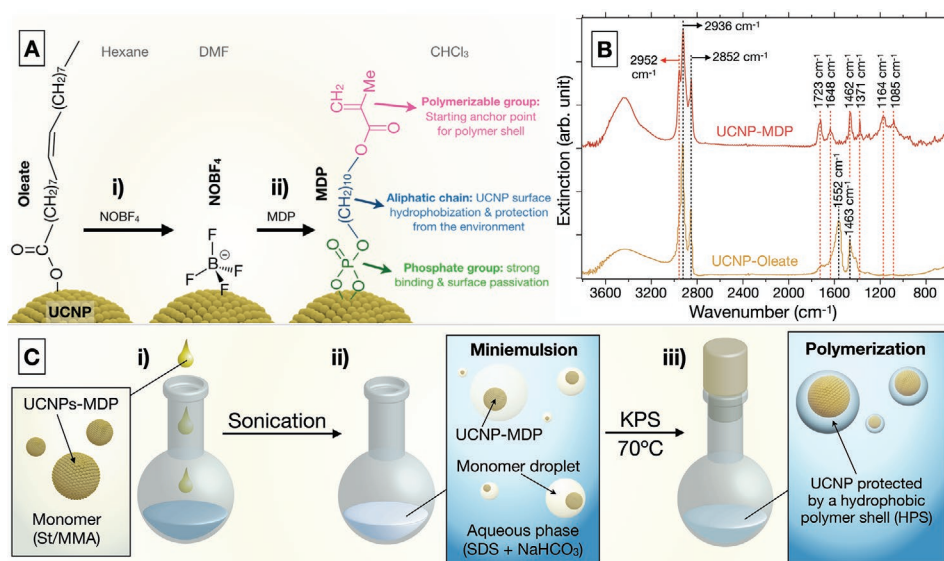
2. Results and Discussion

2.1. Synthesis of UCNPs and Functionalization with MDP

The synthesis of $\beta\text{-NaY}_{0.78}\text{F}_4\text{:Yb}_{0.20}\text{,Er}_{0.02}$ was performed according to a previously reported thermal coprecipitation method.^[43] The adapted protocol described in the Experimental Section yielded monodisperse UCNPs. The mean diameter of the synthesized UCNPs used in this work was 36 ± 1 nm. A representative TEM picture of the resulting $\beta\text{-NaY}_{0.78}\text{F}_4\text{:Yb}_{0.20}\text{,Er}_{0.02}$ UCNPs is depicted in Figure S1A, Supporting Information, showing their monodisperse size distribution and quasi-spherical morphology. HR-TEM analyses (Figure S1B, Supporting Information) shows the crystalline structure of the synthesized UCNPs, with a characteristic lattice distance of 0.52 nm that can be assigned to (100) lattice plane of the hexagonal $\beta\text{-NaYF}_4$.^[44] SAED analysis further confirmed that $\text{NaY}_{0.78}\text{F}_4\text{:Yb}_{0.20}\text{,Er}_{0.02}$ UCNPs were in their β -phase according to the JCPDS 16-0334 diffraction card (Figure S1C, Supporting Information).

The subsequent treatment of UCNPs with NOBF_4 removed from their surface the oleate molecules (Scheme 1A[i]), allowing the phase transfer of the resulting UCNPs from hexane to N,N-Dimethylformamide (DMF). Their later incubation with MDP in DMF/CHCl_3 resulted in their surface functionalization with MDP (Scheme 1A[ii]), as demonstrated by FT-IR analyses (see Scheme 1B). FTIR analyses of the initial oleate-capped UCNPs yielded the characteristic peaks from the asymmetric

and symmetric stretching vibrations of the COO^- group at 1463 and 1552 cm^{-1} , respectively.^[45,46] The additional peaks present at 2852 and 2936 cm^{-1} correspond to the symmetric and asymmetric stretching vibrations of the oleate aliphatic chain, respectively.^[45] Interestingly, after completing the process of ligand exchange with MDP, major changes in the FTIR spectra of UCNPs can be observed: 1) New peaks appear at 1085 and 1164 cm^{-1} corresponding to the $\text{P}=\text{O}$ stretching vibration, when substituted with $-\text{O}-$, and the in-phase stretch vibration of the $\text{P}-\text{O}^-$, 2) the peaks at 1648 and 1723 cm^{-1} evidence the presence of the methacryloyl moiety within the MDP, as these correspond to the stretching vibration of $\text{C}=\text{C}$ conjugated to carbonyl groups and of $\text{C}=\text{O}$ conjugated groups, respectively, 3) the peaks at 2852, 2936, and 2952 cm^{-1} are assigned to the symmetric and asymmetric CH_2 stretching, and the CH_2-O asymmetric stretching from the ether within MDP, respectively.^[45] The ligand exchange with MDP provides the resulting UCNPs with several advantages, see Scheme 1A. First, the phosphate group within MDP has a strong binding affinity toward the surface of UCNPs,^[35] ensuring that the ligand does not detach easily, while providing surface passivation. Second, the MDP aliphatic chain provides hydrophobicity to the surface, which allows UCNPs to be dispersed in the hydrophobic monomer precursors (i.e., St and MMA) that will be polymerized to yield the protective polymer shell in later steps. The MDP aliphatic chains also hamper the adsorption of polar molecules onto the UCNPs' surface, minimizing the luminescence quenching produced by water. Third, the MDP methacryloyl moiety will provide a starting point to initiate, propagate, or terminate the growth of polymer chains during the formation of the protective polymer shell. Finally, MDP can also improve the wetting of UCNPs with polystyrene (PS) and other hydrophobic polymers, favoring a more homogeneous growth of the polymer shell barrier around them and a complete coating of their surface.



Scheme 1. A) UCNPs' surface functionalization process involving i) the removal of oleate capping agent with NOBF_4 and ii) the functionalization of UCNPs with MDP in CHCl_3 . For further details, see Experimental Section. B) FT-IR spectra of the UCNPs capped with oleate and MDP. C) Main steps required to coat UCNPs-MDP with the HPS through miniemulsion polymerization. Namely, i) dropwise addition of UCNPs-MDP dispersed in the monomer (St or St/MMA mixtures) onto the aqueous phase containing SDS and NaHCO_3 ; ii) ultrasonication of the mixture to produce the nanodroplets (i.e., miniemulsion); iii) addition of radical initiator (KPS) and initiation of the polymerization by heating at 70 °C.

2.2. Coating of UCNPs with HPS by Miniemulsion Polymerization

Miniemulsion polymerization was used to coat the resulting UCNPs-MDP with a protective hydrophobic polymer shell (HPS). In this method, St, or a mixture of St and MMA, formed the dispersed oily phase; sodium dodecyl sulfate (SDS) was used as surfactant; hexadecane was used as hydrophobe or droplet costabilizer; and potassium persulfate (KPS) was used as the radical initiator.^[47,48] Miniemulsion polymerization was chosen as the coating method since it offers several advantages compared with other polymerization approaches such as fast polymerization kinetics, high St conversions, the possibility to encapsulate single or multiple nanoparticles (NPs) thanks to their isolation in monomer nanodroplets (i.e., nanoreactors), and a relatively easy control of the polymer shell composition, thickness, and morphology.^[47–52]

Interestingly, if oleate-capped UCNPs are directly used in this polymerization process, uncoated snowman-like Janus structures are obtained due to the partial phase separation between the polymer shell and the nanoparticle during polymerization (see Figure S2, Supporting Information). This was one of the reasons to substitute oleate by a potentially more suitable moiety such as MDP.

The coating of UCNPs-MDP by miniemulsion polymerization is summarized in Scheme 1C. First, UCNPs-MDP were dispersed in St or St/MMA mixtures, and added dropwise to a vigorously stirred aqueous solution of 40 mM SDS and 1.2 mM NaHCO₃, see Scheme 1C[i]. After stirring for 1 h, the resulting emulsion was ultrasonicated to reduce the size of the monomer droplets down to the nanometric range, see Scheme 1C[ii]. This allows to create independent nanoreactors containing the UCNPs-MDP, where the polymerization can start in parallel to encapsulate the UCNPs contained thereof.^[49] After heating the solution to 70 °C, KPS was added to start the radical polymerization of the monomer droplets, yielding the PS or polystyrene-co-poly-methyl methacrylate (PS/PMMA) HPS, see Scheme 1C[iii].

By studying the miniemulsion polymerization process we were able to optimize the coating of the UCNPs-MDP (see Figure 1). Table S1, Supporting Information, summarizes the synthetic conditions tested in this work. First, we confirmed that ultrasonication is essential to form the monomer nanodroplets where the encapsulation of UCNPs-MDP takes place. In the absence of sonication, large submicrometric aggregates of nanoparticles are generated, with poor control of their morphology, as seen in Figure 1P1. On the contrary, the high energy introduced into the system by using an ultrasonication tip (Scheme 1C[ii]) permitted to disrupt and increase the specific surface area of the dispersed phase (i.e., monomer + UCNPs-MDP) in the original emulsion, yielding homogeneous monomer nanodroplets.^[47,49] These were effectively stabilized by hexadecane and SDS molecules,^[47] allowing the polymerization to proceed within these nanoreactors, and resulting in well-defined nanometric HPSs, see Figure 1P2. We additionally tested that ultrasonication baths were able to yield similarly excellent results, making this method more easily accessible by commonly available laboratory instrumentation (see Figure S3, Supporting Information). The adjustment of

the UCNPs-MDP concentration within the dispersed phase, when a fixed amount of SDS and monomer is used, allowed the control of the number of encapsulated UCNPs. Thus, by reducing 4-fold the amount of NPs used during the miniemulsion polymerization, a transition from multi-core shell to single-core shell nanoparticles could be achieved, see Figures 1P2 and 1P3, respectively. The partially eccentric location of the core relative to the shell is ascribed to the interfacial tension between the surface of UCNPs-MDP, the monomer/growing polymer shell, and the aqueous phase.^[51–54] The resulting UCNPs-MDP coated with PS, or “UCNPs@PS” from now on, were monodisperse in size, featuring 88 ± 4 nm in diameter. In order to reduce light scattering produced by these UCNPs@PS (see dispersion and DLS analyses in Figure S4A[i],B,D, Supporting Information), the PS shell thickness was optimized. As a first strategy, the volume of monomer used for the miniemulsion polymerization was reduced from 1.2 to 0.6 and to 0.3 mL (Figures 1P4, 1P5, and 1P6, respectively). This reduced the mean diameter of UCNPs@PS from 88 ± 4 , to 70 ± 5 , and to $60 \text{ nm} \pm 5$ nm, respectively. Interestingly, when the ratio of SDS/monomer is increased upon reducing the amount of monomer, we observed that the lower volume tested (0.3 mL of St, Figure 1P6) was accompanied by an increase of multi-core UCNPs@PS (23.8%) in comparison with only an $\approx 4.8\%$ of multi-core NPs in P5 (0.6 mL of St). This can be explained by the increase in the UCNPs/monomer ratio upon reducing the monomer volume, resulting in an effective increase in the UCNPs concentration. After selecting 0.6 mL as the optimal amount of monomer, we tested the effect of the polymerization reaction time to tune the PS shell thickness (Figure 1P7₁₅–P7₆₀). The polymerization was stopped by quenching the flask in an ice-bath at 15, 30, and 60 min after initiation. This method allowed further control of the size of the UCNPs@PS from 48 ± 5 , to 63 ± 4 , and 70 ± 5 nm (Figures 1P7₁₅, 1P7₃₀, and 1P7₆₀, respectively). Longer reaction times did not substantially increase the final diameter of the UCNPs@PS under the tested conditions. The smallest size obtained tended to aggregate, which is ascribed to the incomplete coating of the UCNPs with PS, resulting in hydrophobic regions that led to interparticle interaction and aggregation in aqueous media. Based on the previous experiments we chose the following conditions as optimal (coating, protection and relatively small size, see Figure S4A[ii],C,E, Supporting Information) to obtain single-core@shell UCNPs@PS: ultrasonication of the sample, 11 mg of UCNPs-MDP, 0.6 mL of St, and 60 min of polymerization reaction time. Finally, modification of the shell composition was explored by varying the monomer concentration added to the reaction from 100 vol% St to 50/50 vol% St/MMA (see Figure 2P100%–P50%). We observed that upon increasing the vol% of MMA, the resulting polymer shells tended to be thinner. In fact, a final diameter of 58 nm was obtained for P75%, while for P50% we obtained the same diameter, 58 nm, after increasing 1.5-fold the initial amount of monomer, see Table S1, Supporting Information. Further increases in MMA vol% (i.e., St/MMA 25%/75%, synthesis P25%) yielded poorer control over the polymer shell thickness, morphology, and polymerization under our tested conditions (see Figure S5, Supporting Information). This can be explained by the increased nucleation and growth of PMMA particles in

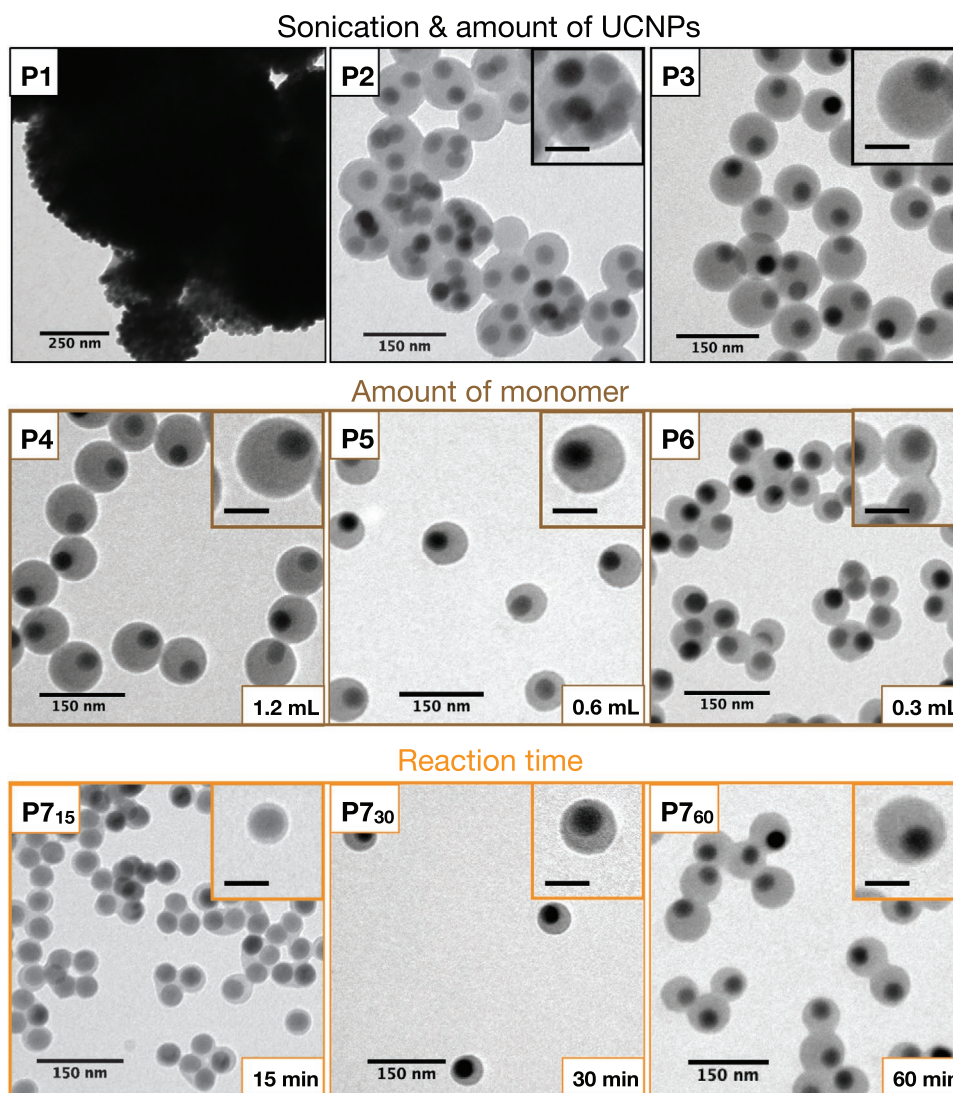


Figure 1. TEM images of: P1) UCNPs@PS aggregates produced when no ultrasonication step is performed; P2) Multi-core@shell UCNPs@PS when incorporating the ultrasonication step into the process. The creation of nanoreactors where polymerization occurs in a confined way is evidenced by the discrete encapsulation of multiple UCNPs; P3) Single-core@shell UCNPs@PS produced after adjusting the initial amount of UCNPs-MDP from 44 to 11 mg. P4–P6) UCNPs@PS produced after adjusting the initial amount of monomer (St) from 1.2 to 0.6 and 0.3 mL, respectively. P7₁₅–P7₆₀) UCNPs@PS produced after quenching the polymerization reaction at 15, 30, and 60 min after initiation, respectively. All main image scale bars = 150 nm; All inset scale bars = 50 nm.

the aqueous phase, due to the higher polarity of MMA in comparison with St.^[55] Still, the incorporation of PMMA to the protective shell was confirmed by FT-IR analyses (see Figure S6, Supporting Information), proving the feasibility to easily incorporate different monomers during the polymerization process in order to vary the shell properties of the resulting UCNPs.

2.3. Comparison of Protective HPS with a Standard Poly-Acrylic Acid Coating

Given the polar nature of the chemicals responsible for the deterioration of UCNPs upon water-transfer, the most effective way to protect them may be to maintain a robust hydrophobic environment near the UCNPs' surface, avoiding the diffusion

of these polar species toward it. This should result in the reduction of all detrimental effects associated with water-transfer of UCNPs, by using one single strategy. In this vein, miniemulsion polymerization has the advantage of isolating UCNPs in hydrophobic nanoreactors (i.e., monomer droplets) until a thick hydrophobic layer of polymer is created, which ensures protection from the aqueous environment, while being negligibly affected by ligand equilibrium due to its solid-like state, contrary to what is expected with other strategies.^[30,36] The surface of the resulting shell is simultaneously decorated with sulfate groups that come from both, chain termination steps with sulfate radicals generated by the initiator (KPS), and SDS surfactant molecules that keep adsorbed after polymerization.^[56–58] Sulfate groups deprotonate within a wide range of pHs (pK_a < 2), providing colloidal stability in water. The presence of

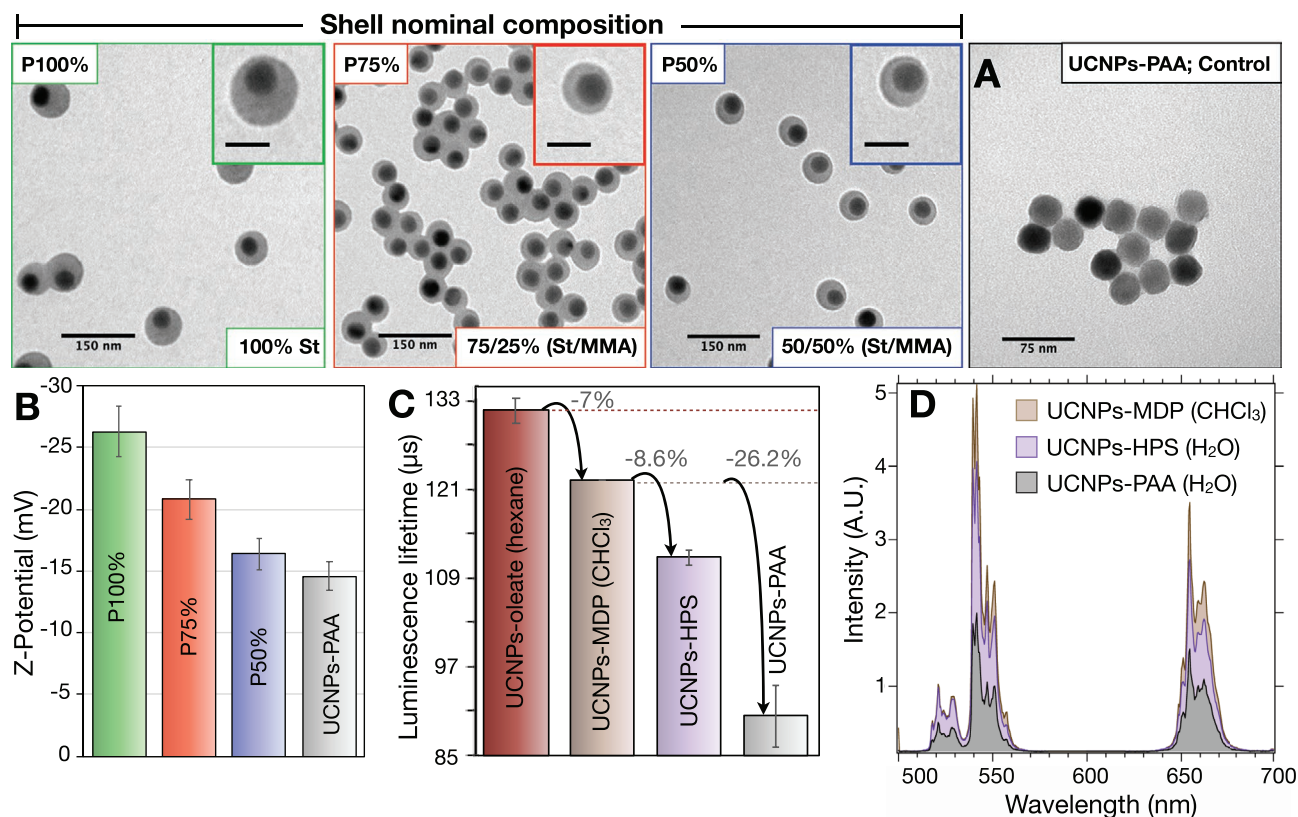


Figure 2. P100%–P50%) TEM images of UCNPs-MDP coated with HPSs with nominal compositions of 100% PS, 75%/25% PS/PMMA, and 50%/50% PS/PMMA, respectively. A) TEM image of UCNPs coated with PAA (control sample). All inset scale bars = 50 nm. B) Z-potential values of P100%, P75%, P50%, and UCNPs-PAA. C) Green emission lifetime values at 540 nm ($^4S_{3/2} \rightarrow ^4I_{15/2}$) of UCNPs-Oleate (hexane), UCNPs-MDP (CHCl₃), UCNPs-HPS (H₂O), and UCNPs-PAA (H₂O). D) Upconversion emission spectra of UCNPs-MDP, UCNPs-HPS, and UCNPs-PAA at 525 nm ($^2H_{11/2} \rightarrow ^4I_{15/2}$; green), 540 nm ($^4S_{3/2} \rightarrow ^4I_{15/2}$; green), and 655 nm ($^4F_{9/2} \rightarrow ^4I_{15/2}$; red). The protection of UCNPs against water quenching by HPSs is further confirmed, yielding approximately 2-fold more intense emissions in comparison with UCNPs-PAA. The UCNP core concentration of UCNPs-MDP, UCNPs-HPS, and UCNPs-PAA was 100 $\mu\text{g mL}^{-1}$ for the C) lifetime and the D) steady-state luminescence measurements.

these highly stabilizing surface charges is demonstrated for all HPSs by Z-potential measurements, as seen in Figure 2B. It is noteworthy that the colloidal stability offered by those surface charges is, in principle, higher than that provided to UCNPs by poly-acrylic acid (PAA), see Figure 2A,B (gray color). PAA is a widely used polydentate ligand for the water-transfer of UCNPs, which provides them with colloidal stability, surface passivation, relative protection in aqueous media, and carboxylic groups that can be used for further bioconjugation.^[25,59] For these reasons, we will compare the optical properties and chemical resistance of our HPS-coated UCNPs with more conventional PAA-coated UCNPs used as a control in previous works, from now on “UCNPs-PAA” (see Figure 2A).^[33,36,42] The substitution of oleate with MDP as capping agent is accompanied by a decrease in the UCNPs’ lifetime of 7% (see Figure 2C), which is ascribed to the change of solvent (from hexane to CHCl₃) and to a slight quenching effect produced by the phosphate moiety contained within the MDP structure (see Scheme 1A). The subsequent water-transfer of UCNPs through miniemulsion polymerization results in another reduction in lifetime (8.6%), probably due to the adsorption of a small number of water molecules onto the UCNP’s surface. Interestingly, different HPS compositions yielded almost the same exact lifetime (see Figure S7, Supporting Information),

indicating that the coating process is not substantially affected by changing the hydrophobic monomer, at least within the tested range of compositions.

In contrast, the water-transfer of UCNPs with the conventional PAA ligand results in a pronounced decrease in lifetime (26.2%) when compared with UCNPs-MDP. This is explained by the high permeability of this polydentate ligand to water molecules, which easily reach the UCNPs’ surface and produce a strong quenching of their luminescence. The effect of the lifetime reduction on the luminescence properties of these UCNPs was also confirmed by steady-state luminescence measurements, as seen in Figure 2D. In fact, the use of HPSs resulted in UCNPs with about 2-fold more intense upconversion luminescence than the same UCNPs coated with PAA (see Figure S8, Supporting Information), which further confirms the effectiveness of our strategy to reduce luminescence quenching in aqueous media.

To further assess the protective role of the HPS and compare it with the PAA shell, we carried out long-term stability studies at RT using aqueous dispersions of UCNPs-HPS at very low concentrations (5 $\mu\text{g mL}^{-1}$), which is well below the concentration at which noticeable degradation of UCNPs appear ($\approx 50 \mu\text{g mL}^{-1}$).^[15] This low concentration allowed us to study the effect of UCNPs dissolution on their optical

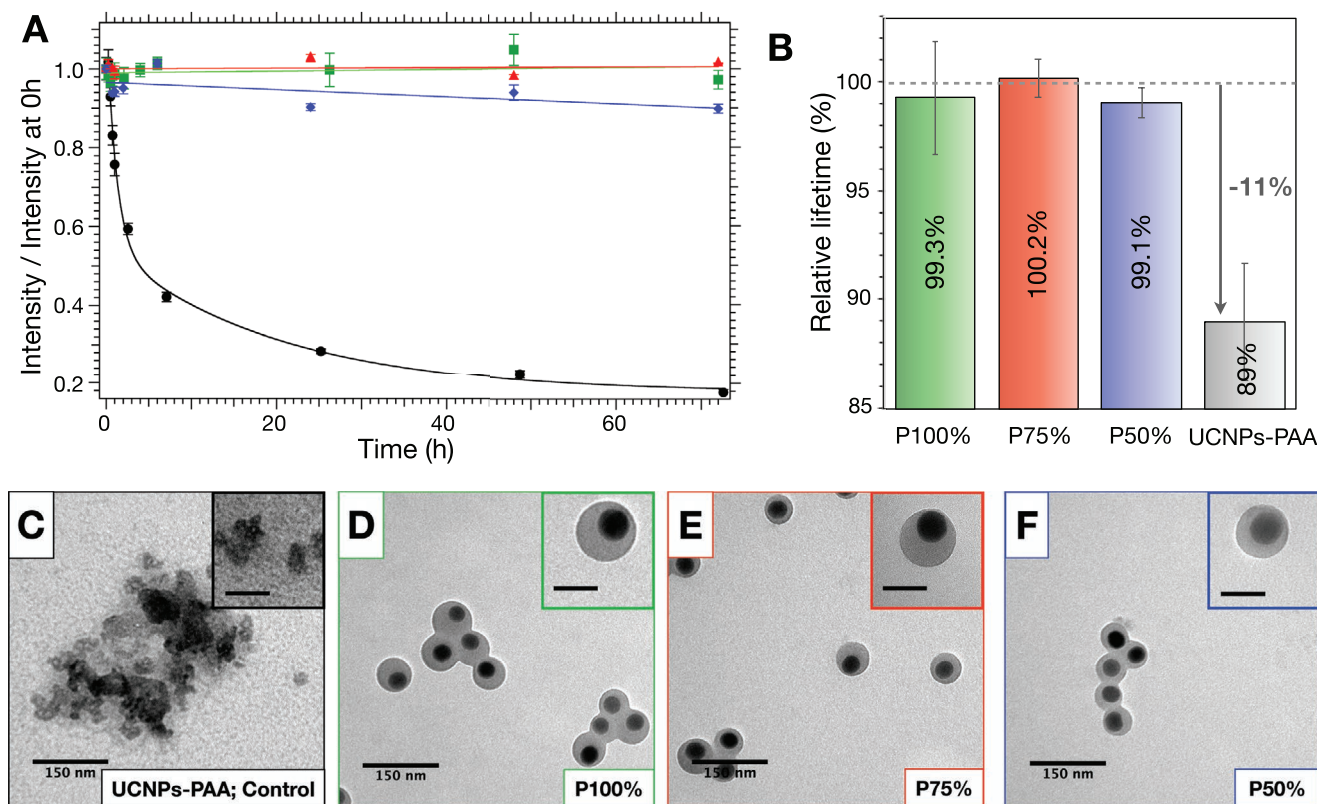


Figure 3. A) Time evolution (0–72 h) of the green upconversion luminescence intensity after dilution of the samples at a core concentration of $5 \mu\text{g mL}^{-1}$. P100% (green), P75% (red), P50% (blue), and UCNPs-PAA (black). B) Relative lifetime change of the green upconversion emission after 72 h, compared with the original lifetime at 0 h. P100% (green bar), P75% (red bar), P50% (blue bar), and UCNPs-PAA (gray bar). C–F) TEM images of UCNPs-PAA, P100%, P75%, and P50%, after 72 h in water at a core concentration of $5 \mu\text{g mL}^{-1}$, respectively. All inset scale bars = 50 nm.

and structural/morphological properties (see **Figure 3**). The degradation of the samples was monitored by following their luminescence intensity for 72 h. **Figure 3A** shows their luminescence intensity normalized to their initial intensity, as a function of time. Samples P100% and P75% did not exhibit any sign of degradation, since their luminescence intensity did not change during the 72 h (see green and red lines, respectively). On the other hand, P50% sample (blue line) showed a slight decrease in luminescence intensity of $\approx 10\%$, which may be ascribed either to a slightly worse colloidal stability, or a less effective protection compared with P100% and P75%. The luminescence from the UCNPs-PAA sample was highly compromised (see black line in **Figure 3A**) especially during the first 3–4 h, with a reduction of 50% in their luminescence intensity, and after that, a slower decrease continued over time up to 80%. **Figure 3B** shows the relative luminescence lifetime change of the samples after 72 h, in comparison with the lifetime value yielded by the original non-aged UCNPs samples. These measurements can be used to confirm structural degradation of UCNPs, as reported by other authors.^[23,46] Our results confirm once again the degradation of UCNPs-PAA (see **Figure 3B**, gray bar), as the 72 h aged NPs are accompanied by a $\approx 11\%$ decrease compared with their original lifetime. Interestingly, the relative lifetime measurements obtained for P100%, P75%, and P50% after 72 h (see **Figure 3B**; green, red, and blue bars, respectively) show negligible changes (less than 1%). These results

clearly highlight the remarkable protection exhibited by the HPS against UCNPs dissolution. This was also corroborated by TEM, where no damage or structural/morphological changes could be found for the UCNPs-HPS (see **Figure 3D–F**), whereas the UCNPs-PAA were strongly affected, as shown in **Figure 3C**. Interestingly, the latter NPs presented a significant reduction of their diameter, from the initial value of 36 nm to a final value of 27 nm. This would mean that the degradation took place at the outer part of the nanoparticle, maintaining the spherical symmetry. After these results, it may seem counterintuitive how the huge relative intensity drops shown by the UCNPs-PAA ($\approx 80\%$) was accompanied by only a modest relative lifetime decrease ($\approx 11\%$). However, this can be explained by the fact that UCNPs-PAA's surface is already highly quenched by water, so further lifetime reductions should be mainly due to an increase in UCNPs' surface-to-volume (S/V) ratio as dissolution progresses. On the contrary, the same dissolution process has a more relevant deleterious effect on the UCNPs intensity, as the physical separation and diffusion of Ln^{3+} from the host matrix implies the reduction of the number of sensitizers (Yb^{3+}) and activators (Er^{3+}) that can produce efficient energy transfer, and ultimately photon upconversion. As a direct consequence, the intensity of upconversion luminescence is highly reduced.

In order to test this hypothesis, we theoretically estimated the reduction of the UCNPs-PAA luminescence intensity by considering the experimentally observed decrease in the

UCNP diameter. Two main contributions were taken into account. First, the reduction of the number of ions present in the UCNPs, which is related to the UCNPs volume. Second, the decrease of the emission efficiency (quantum yield or lifetime) of the UCNPs-PAA due to surface quenching effects as the nanoparticle S/V ratio increased. These two effects allowed us to properly reproduce the intensity drop of these nanoparticles (see Figure S9, Supporting Information). Interestingly, this allowed us to confirm that the main contribution came from the ion dissolution, since more than 50% of ions were estimated to be lost. This result helps to explain why the degradation of the UCNPs showed a smaller decrease in the lifetime than in the luminescence intensity. Furthermore, the reduction in UCNPs size during dissolution was predicted to follow a logarithmic relationship with time, matching quite accurately the experimental data. We also estimated the solubility product $K_{sp} = [Na^+][RE^{3+}][F^-]^4$, where RE^{3+} represents the rare-earth ions Y^{3+} , Yb^{3+} , and Er^{3+} . For this, we assumed that ions dissolved stoichiometrically. The experimental results (TEM images) showed a mean final diameter below 27 nm which could be related to a RE^{3+} ion dissolution near to 70%. Therefore, the RE^{3+} ion equilibrium concentration was 0.7 times the concentration of RE^{3+}

ions in the sample, being 0.0266 mM for a $5 \mu\text{g mL}^{-1}$ of UCNPs. Therefore, the computed solubility product was $K_{sp} = 1 \times 10^{-26}$ which roughly agrees with previous values.^[15]

We also studied the stability of very diluted samples of UCNPs ($5 \mu\text{g mL}^{-1}$) with different protective shells in potassium phosphate buffer (K^+PB) at a concentration of 100 mM, which is ten times higher than common phosphate buffer saline. This buffer quickly and completely degraded the control sample UCNPs-PAA, as can be observed by the 50% luminescence reduction after 1 h and the almost complete disappearance of upconversion luminescence after 72 h (Figure 4A, black line). The reduction in luminescence was such that it was impossible for us to measure the resulting lifetime of the sample (Figure 4B), indicating a profound degradation of the UCNPs host matrix and its structure. HR-TEM characterization further confirmed the complete degradation of UCNPs-PAA by K^+PB , yielding a new inorganic phase with an acicular and entangled morphology (see Figure 4C[i]). Characterization of the sample by HAADF-TEM indicates the presence of clusters containing atoms of high atomic number (brighter regions), probably traces of aggregated UCNPs-PAA, from which the acicular structures seem to originate. EDX elemental mapping analyses confirm

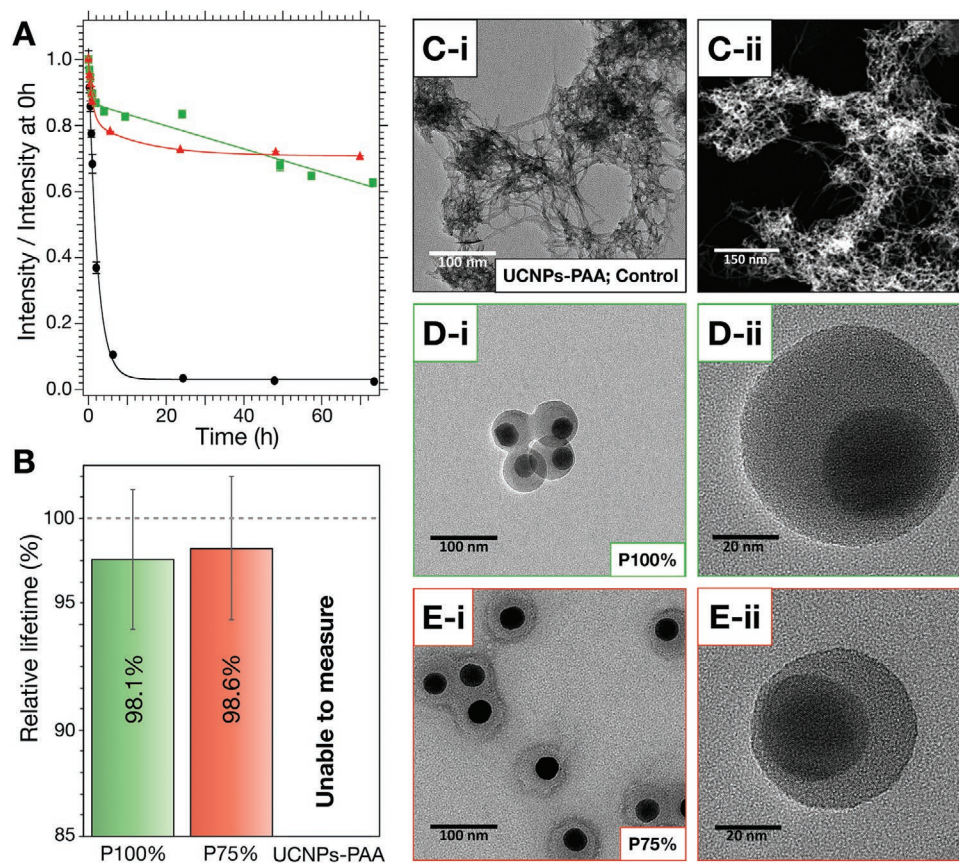


Figure 4. A) Time evolution (0–72 h) of the green upconversion luminescence intensity after dilution of the samples to a core concentration of $5 \mu\text{g mL}^{-1}$ in concentrated K^+PB (100 mM). P100% (green), P75% (red), and UCNPs-PAA (black). B) Relative lifetime change of the green upconversion emission after 72 h at $5 \mu\text{g mL}^{-1}$ in concentrated K^+PB (100 mM), compared with the original lifetime at 0 h. P100% (green bar), P75% (red bar), and UCNPs-PAA (gray bar). HR-TEM images of C[i] UCNPs-PAA, D[i,ii] P100%, and E[i,ii] P75% after 72 h in K^+PB (100 mM) at a core concentration of $5 \mu\text{g mL}^{-1}$, respectively. C[ii] HAADF-STEM image of UCNPs-PAA, where the brightest regions within the material are likely to contain atoms of higher atomic number.

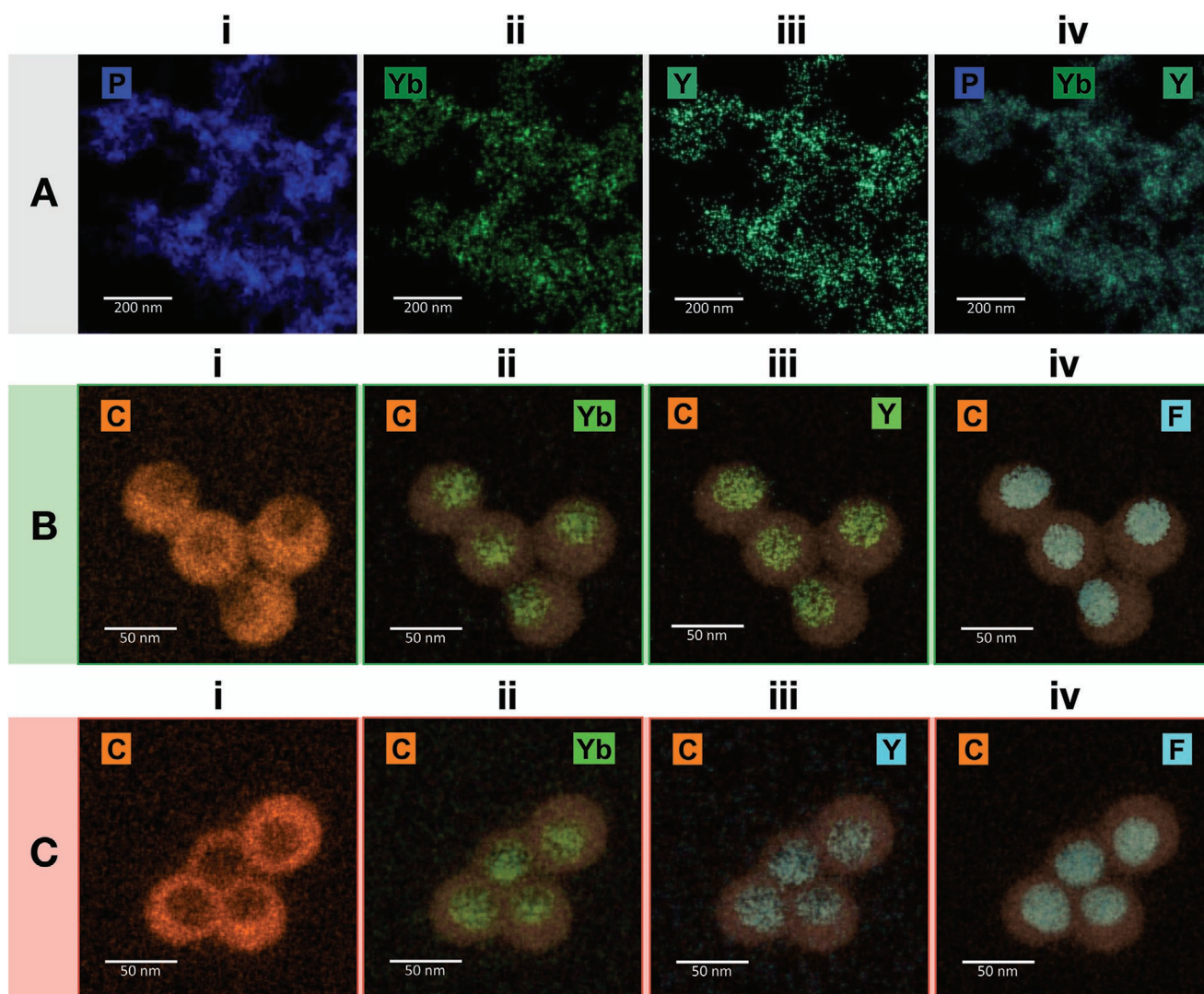


Figure 5. EDX elemental mapping analyses of A) UCNPs-PAA, B) P100%, and C) P75%. (A[i–iv]) corresponds to the signals from elements in UCNPs-PAA: A[i] phosphorous, A[ii] ytterbium, A[iii] yttrium, A[iv] Merged image of phosphorus, ytterbium, and yttrium. Scale bar in (A[i–iv]) is 200 nm. (B[i–iv]) corresponds to the elements in P100%: B[i] carbon, B[ii] ytterbium, B[iii] yttrium, and B[iv] fluorine. (C[i–iv]) corresponds to the elements in P75%: C[i] carbon, C[ii] ytterbium, C[iii] yttrium, and C[iv] fluorine. Scale bar in B[i–iv] and in C[i–iv] is 50 nm.

the presence of phosphorus (P), ytterbium (Yb), and yttrium (Y) in these structures (see **Figure 5A**[i], **5A**[ii], and **5A**[iii], respectively). Noteworthy, the merged image in **Figure 5A**[iv] reveals a spatial correlation between these elements, suggesting that the new phase formed upon UCNPs degradation is composed of a complex mixture of RE phosphates. Most interestingly, we could not detect the presence of fluorine (F) in this sample, suggesting the complete degradation of UCNPs-PAA upon reaction with phosphate and the release of all fluoride ions (F^-) to the medium in the form of soluble species (e.g., NaF and/or KF). These observations match the results reported in previous works.^[23,46] The multiple centrifugations performed prior to HR-TEM characterization, aiming to remove excess K^+PB , may have washed away these water-soluble F^- species, which explains the total absence of fluorine signal during EDX elemental mapping analyses. More detailed comparative elemental analyses can be found in **Figure S10**, Supporting Information.

As opposed to UCNPs-PAA, the long-term luminescence intensity study of P100% and P75% presented a much lower, but still moderate, drop in their upconversion luminescence after 72 h (37% and 29% reduction, see **Figure 4A** green and red symbols, respectively). Nevertheless, when measuring their relative lifetime change, an almost negligible 1.9% and 1.4% decrease was found (**Figure 4B** green and red bars, respectively). This suggests that most UCNPs are well protected and preserve their luminescence properties in K^+PB . Nevertheless, K^+PB forms less soluble potassium SDS salts, and is used in similarly high concentrations in biochemistry protocols to reduce the solubility of SDS, which in our case acts as colloidal stabilizer at the surface of the HPS.^[60,61] This could indeed explain the almost negligible change in the lifetime, but a moderate reduction in luminescence intensity. To further test this hypothesis, we confirmed by DLS that the hydrodynamic diameter (D_H) of P100% and P75% increased in K^+PB compared with the results

obtained in DI-H₂O, which can be ascribed to a reduction of the interparticle distance due to a decrease in colloidal stability, see Figure S11, Supporting Information. Although this is certainly undesirable, the results from UCNP-HPS in K⁺PB represent a huge improvement in comparison with more traditional coatings, such as UCNP-PAA. In order to fully confirm the morphological and structural integrity of P100% and P75%, we performed HR-TEM characterizations of the samples after 72 h aging in K⁺PB. Figure 4D[i,ii],E[i,ii] confirmed that the morphology of P100% and P75% has not been affected after 72 h in K⁺PB. The quasi-spherical shape of the UCNP cores is conserved, while no sign of the acicular structures formed from the reaction between phosphate and RE³⁺ is detected (see Figure 4C[i,ii] for comparison). A closer look to P100% and P75% (Figure 4D[ii],E[ii]) further confirmed that no degradation of UCNP cores was present, even at the regions of thinner HPS coating. Higher magnification of these images showing the conserved crystallinity of the NPs can be seen in Figure S12, Supporting Information, where the lattice planes can be noticed. These images provide initial evidence to support that an HPS shell thickness as thin as 3–4 nm may be enough to fully protect UCNPs in aqueous media against chemical degradation (see Figure S12, Supporting Information). As a final chemical and structural characterization, we performed EDX elemental mapping of P100% and P75% (see Figures 5B and 5C, respectively). A strong signal from carbon could be observed in the region corresponding to the HPS, while a void was noticeable at its core, due to the presence of the inorganic UCNP (Figure 5B[i],C[i]). Within this region, yttrium, yttrium, and fluorine could be identified, matching very nicely the area corresponding to the UCNP core in both samples, see images of Yb, Y, and F merged with carbon in 5B[ii], 5B[iii], and 5B[iv] (for P100%), and 5C[ii], 5C[iii], and 5C[iv] (for P75%), respectively. The high signal obtained from these elements at the UCNP core region is strong evidence that the HPS prevents the leaking of ions from the UCNP toward the solution and their later reaction with phosphate. In fact, the case of fluorine is specially revealing, since its high abundance in the core of P100% and P75% suppose a high contrast regarding the total

absence of this signal in UCNP-PAA, where the whole fluoride has been exchanged by phosphate after 72 h in K⁺PB (see Figure 5A[i,iv]). Quite interestingly, we could detect the presence of the MDP ligands at the surface of UCNP cores, within the HPS, as this is the only possible source of phosphorus that can be present at the UCNP core surface before putting them in contact with K⁺PB (see Figure S13, Supporting Information). To further verify that MDP was being detected, we also confirmed that phosphorus signal was absent in UCNP-PAA before ageing in K⁺PB (data not shown). The detection of MDP suggests that the growth of the HPS, apart from providing a robust hydrophobic barrier, serves to ensure the long-term passivation of the surface by keeping the phosphate moieties from MDP molecules in place. For further compositional analyses of P100% and P75% after 72 h incubation in K⁺PB see Figures S14A and S14B, Supporting Information, respectively. Overall, our results indicate that HPS offers great protection against water quenching, ion leaking and dissolution, and chemically harmful species such as phosphate.

Aiming to reliably expand the current applications of UCNP, we explored the potential of HPS as a protecting layer under high-temperature conditions in aqueous media. Thus, we studied the stability of UCNP in DI-H₂O at 70 °C and high dilution (5 μg mL⁻¹). Again, the HPS offered a much higher protection against degradation than the PAA shell. In fact, UCNP-PAA are completely degraded in the first 3 h, dropping their luminescence intensity a 90% (see Figure 6A, black). In contrast, P75%, which was selected for yielding the best results in the previous experiments, showed only a 20% reduction (red in Figure 6A). Although this is not a negligible reduction, it is important to highlight that the intensity of P75% after 7 h at 70 °C is still even higher than that from undegraded (non-aged) UCNP-PAA at the same concentration. The undetectable luminescence signal obtained for the UCNP-PAA sample after 7 h at 70 °C made it impossible to determine its lifetime. In contrast, the lifetime remains almost unchanged for P75% (drop ≈ 3%), see red bar in Figure 6B. This can indicate that the reduction of their luminescence could possibly be ascribed to a very low but non-negligible quenching or degradation of a

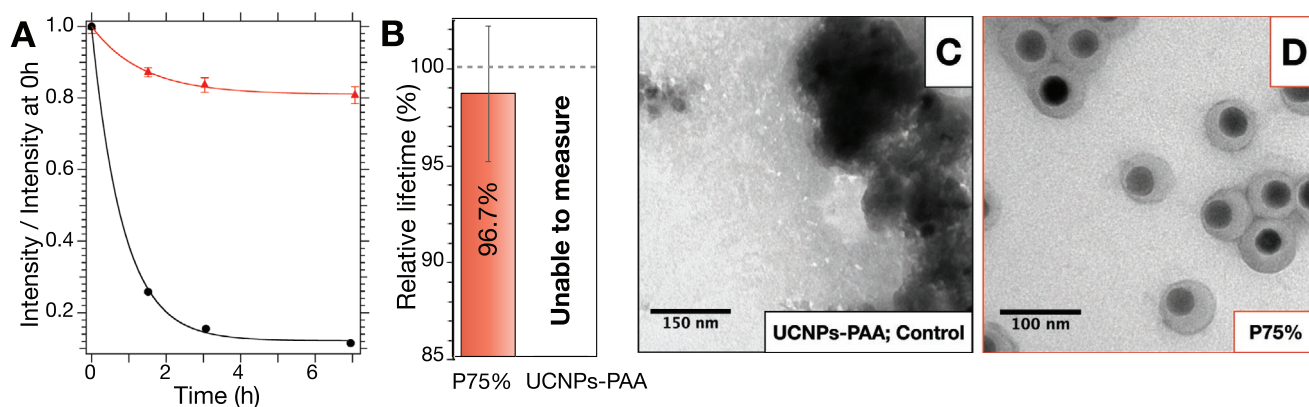


Figure 6. A) Time evolution (0–7 h) of the green upconversion luminescence intensity of the samples with a core concentration of 5 μg mL⁻¹ in DI-H₂O at 70 °C. P75% (red) and UCNP-PAA (black). B) Relative lifetime change of the green upconversion emission after 72 h at 5 μg mL⁻¹ in DI-H₂O at 70 °C, compared with the original lifetime at 0 h. P75% (red bar) and UCNP-PAA (gray bar). C,D) HR-TEM images of UCNP-PAA, and P75% after 7 h in DI-H₂O at 70 °C.

small fraction of P75%. We hypothesize that upon increasing the temperature to 70 °C, the thinnest shell regions can become partially permeable, allowing some H₂O molecules to reach the UCNPs' surface in a small population of UCNPs-HPS. Still, TEM characterization revealed that, whereas UCNPs-PAA were completely degraded and aggregated due to dissolution/precipitation processes (Figure 6C), P75% showed that the HPS effectively protected UCNPs cores even under these extreme conditions (see Figure 6D and Figure S15, Supporting Information, for more TEM images). In fact, no sign of particle degradation could be observed by TEM, which may indicate that only a very small fraction of UCNPs-HPS is partially affected. These results are very exciting, considering that they open the possibility to more reliably use UCNPs-HPS in novel applications such as high temperature nanothermometry, nucleic acid amplification techniques such as PCR, or isothermal approaches. A demonstration of the thermometric properties of P75% can be found in Figures S16 and S17, Supporting Information, where the sensitivity exhibited by P75% is comparable to the values found in literature for β -NaYF₄:Yb,Er nanothermometers.

As already mentioned, most proposed strategies aim to avoid degradation by using capping agents or polydentate ligands with high binding affinities, sometimes in a multilayer fashion, to passivate their surface and limit the diffusion of ions.^[33,35,42,62,63] Nevertheless, it is important to highlight that these ligands inherently show a hydrophilic character (e.g., PEG-phosphate, poly-phosphates, poly-phosphonates, PAA, and poly-sulfonates), necessary to provide UCNPs with the pursued water dispersibility. This implies that they may be usually accompanied by: 1) a certain degree of water permeability, and 2) unprotected surface regions due to incomplete coating.^[15,30,36] Thus, although these strategies effectively delay the detrimental effects associated to water-transfer, they can be expected to eventually permit the diffusion of water and other small-sized polar molecules toward the surface of the UCNPs, and to the very inner regions of their host matrix as degradation starts, especially in high dilution and non-steady conditions.^[15,36] A shocking example of this permeability can be observed in the dissolution of UCNPs coated with silica shells, even when these shells are thick and robust, which can be explained by a certain degree of porosity exhibited by these hydrophilic coatings.^[13,15] Only super thick silica shells has recently proved to protect UCNPs at concentrations of 50 $\mu\text{g mL}^{-1}$ along a period of 72 h in aqueous media, including phosphates, which represents a significant advance compared with previous attempts, although at the sacrifice of its final size (≈ 166 nm in diameter).^[25]

Based on our results, the best way to solve these issues is, to our eyes, maintaining a protective hydrophobic environment surrounding the UCNPs, as this will simultaneously cancel all these detrimental mechanisms. In fact, a very recent work by Märkl et al. also points in this direction, by isolating UCNPs with phospholipid bilayers, showing very promising results in different media, including phosphate buffers.^[64] In this regard, our strategy has proven to be remarkably effective: all experiments have been performed at very low concentrations (5 $\mu\text{g mL}^{-1}$; similarly to those used in ultrasensitive bioassays), and, on top of this, under extremely aggressive conditions such as highly concentrated K⁺PB (100 mM) and high temperatures

(70 °C). In-depth characterizations provided strong evidence that HPSs offer a simultaneous solution to all problems associated with water-transfer of UCNPs, namely, water-quenching, dissolution/leaking, and degradation through reaction with chemically aggressive species such as phosphates. Although further bioconjugation of UCNPs-HPS was out of the scope of the present work, different chemical approaches may be used to address this issue. Among them, layer by layer deposition,^[65] growing of a thin layer of organosilane,^[66,67] or adding functional monomers during the polymerization (e.g., acrylic acid) are interesting strategies to explore in the future.^[68,69] The miniemulsion polymerization approach developed herein stands out as a very versatile and affordable approach, which also allows straightforward TEM characterization of the quality and thickness of the resulting HPS coating. Thus, we are convinced that the proven advantages of this strategy, combined with the room for creating exciting new optical and multifunctional systems by embedding additional NPs or moieties within the HPS, will prompt the development of a new wave of lanthanide-doped materials with novel functionalities, as well as with enhanced properties and reliability. A list of nanomaterials that may benefit from our approach is presented in Table S2, Supporting Information.

3. Conclusion

In this work, we have developed a new methodology to help solve all detrimental effects associated with the transfer of UCNPs to aqueous media. We successfully combined two strategies: 1) the substitution of oleate by MDP as capping agent, to achieve higher binding affinity, hydrophobic surface properties, and polymerizable groups; and 2) the growth of a robust HPS around the UCNPs to provide long-term and effective protection from the environment. Fine tuning of the number of encapsulated UCNPs, shell thickness, and composition (PS, and PS/PMMA HPS) was demonstrated. Strong evidence of the high protection produced by this HPS against water quenching, dissolution, and degradation by phosphates is shown, even at an atomic level. This was proven under extremely aggressive conditions for UCNPs (high dilution combined with high phosphate concentration or high temperature) and was even more remarkable upon comparison with the very high degradation suffered by UCNPs coated with PAA, used as a control sample. Results from the study on the dissolution of UCNPs-PAA allowed us to theoretically estimate and understand the origins of their luminescence drop. We attributed most of this effect to the release of Ln³⁺ from the host matrix to the environment, while a smaller contribution stems from the loss of quantum efficiency as the S/V ratio of UCNPs increases during dissolution, being this last effect responsible for the lifetime luminescence decrease. This also permitted us to roughly calculate the solubility K_{sp} of β -NaYF₄. Finally, we have successfully confirmed the protective role of HPS in aqueous media at 70 °C. This lays the foundations to reliably expand the use of UCNPs, or more generally of lanthanide-doped NPs coated with HPS, as reporters in applications that involve high temperatures such as sensing platforms relying on real-time PCR and isothermal amplification strategies. Additionally, their use as luminescent

nano-thermometers that can provide a reliable thermal feedback in these techniques, especially when incorporated to microfluidic platforms, or during hyperthermal and photothermal ablation therapies, may also prove to be a valuable tool. Overall, the proposed strategy stands out as a promising and versatile solution, not only for UCNPs, but potentially for other NPs that may experience similar problems upon water-transfer. More interestingly, it offers room for a new generation of multifunctional materials, by taking advantage of the possibilities related to embedding additional moieties within the HPS.

4. Experimental Section

Further details concerning the materials and methods used in this work can be found at the Materials and Methods Section in Supporting Information.

Synthesis of β -NaY_{0.78}F₄:Yb_{0.20}:Er_{0.02} (UCNPs): The synthesis of β -NaYF₄:Yb_{0.20}:Er_{0.02} was carried out by the thermal coprecipitation method in organic media with some modifications.^[43] First, YCl₃ · 6H₂O (236.63 mg, 0.78 mmol), YbCl₃ · 6H₂O (77.47 mg, 0.20 mmol), and ErCl₃ · 6H₂O (7.63 mg, 0.02 mmol) were dissolved in 1 mL of MeOH. Then, this solution was added to a 100 mL three-necked round bottom flask, which contained oleic acid (OA; 6 mL, 19 mmol) and 1-octadecene (ODE; 15 mL, 46.9 mmol). The resulting flask content was stirred while heated up to 140 °C under nitrogen (N₂) flow with a heating rate of 5 °C min⁻¹. Next, the temperature was maintained for 20 min while the flask was connected to a vacuum pump, in order to remove the traces of water, methanol, and hydrochloric acid. After that, the flask was let to naturally cool down to RT. Then, a freshly prepared 10 mL methanol solution containing NaOH (100 mg, 2.5 mmol) and NH₄F (148.16 mg, 4.0 mmol) was added under moderate stirring into the flask containing the dissolved rare earths. The resulting content was mixed for 30 min at 30 °C. Then, the mixture was heated up to 110 °C (4 °C min⁻¹) under an N₂ atmosphere and kept for 20 min under vacuum to remove solvent traces. After that, the mixture was heated to 315 °C at 16 °C min⁻¹ and kept at this temperature for 1 h. Later, the reaction was allowed to cool down to RT, and the resulting UCNPs were split into four centrifuge tubes. Then, 4 mL of methanol was added to each tube, shaken, and let to separate. The methanol phase was removed, and this process was repeated twice. Next, the product was centrifuged at 7500 × g for 20 min. Once centrifuged, the supernatant was discarded and the pellets were rinsed, without dispersing them, using 2 mL of ethanol. This process was repeated once. Finally, the pellets were dried at RT for 2 min, dispersed in 4 mL of hexane, and stored for further experiments.

Removal of UCNPs' Capping Agent: The removal of oleate (capping agent) from the UCNPs' surface was performed by a slightly modified method.^[70,71] In brief, 8 mL of DMF was added to a 50 mL round bottom flask containing a magnetic stirring bar. Next, 100 mg of UCNPs in hexane was ultrasonicated for 5 min, and carefully added on top of the DMF phase, with no stirring. Then, 100 mg of NOBF₄ was added into the flask, and the two phases were mixed for 10 min under vigorous stirring. The removal of the majority of oleate molecules from the UCNPs' surface was confirmed by their phase transfer, from hexane to DMF. According to previous reports, a 15–20% of oleate could still remain attached to the surface after this treatment.^[70] The DMF phase was then extracted and split into two Teflon centrifuge tubes, which were completed by adding CHCl₃ and centrifuged at 10 000 × g for 10 min. Next, each pellet was redispersed in 1 mL of DMF and the centrifuge tubes were completed with 7 mL of CHCl₃ and centrifuged again. This process was repeated twice more. Finally, the UCNPs were redispersed in 2 mL of DMF and stored.

Surface Functionalization of UCNPs with MDP: First, 53 mg of MDP (0.17 mmol) were introduced in a glass vial containing a magnetic stirring bar. Then, 10 mL of CHCl₃ were added, and the mixture was stirred vigorously until MDP was completely dissolved. The amount of

MDP was always adjusted so that a theoretical surface coating excess corresponding to ≈25 MDP molecules per nm² of UCNPs was achieved. At this point, 2 mL of uncapped UCNPs (50 mg mL⁻¹) in DMF was introduced into the vial, ultrasonicated for 2 min, and let to incubate under moderate stirring for 1 h. Then, the resulting UCNPs-MDP dispersion was split into two Teflon centrifuge tubes, 600 μL of hexane was added on top of each one, and they were centrifuged at 13 300 × g for 12 min. Next, the supernatant was carefully discarded, the pellets were redispersed in 7 mL of CHCl₃, 600 μL of hexane were added, and the tubes were centrifuged again. This washing process was repeated a total of three times. Finally, the pellets were redispersed in 3 mL of CHCl₃ and stored at 4 °C in a sealed vial. The concentration of the resulting dispersion, as well as the UCNPs-MDP inorganic/organic weight %, was typically determined by weighting the dry product of a known volume in a precision balance, and by thermogravimetric analysis (TGA). See TGA in the Methods Section in Supporting Information for further details.

Polymerization of UCNPs-MDP to Obtain Protective Hydrophobic Polymer Shells: In a typical synthesis, 11 mg of UCNPs-MDP in CHCl₃ was centrifuged at 21 000 × g for 10 min. The supernatant was discarded, and the CHCl₃ traces were removed from the pellets by using a gentle airflow. The resulting pellet was redispersed in 600 μL of St by ultrasonication and centrifuged again. Next, the pellet was redispersed in 600 μL of St by ultrasonication (2 min), 7.2 μL of hexadecane was added, and the dispersion was vortexed and ultrasonicated by 2 min. The dispersion was then added dropwise into a 10 mL round bottom flask containing 4.5 mL of SDS (40 mM) and NaHCO₃ (1.2 mM) under vigorous stirring, the flask was capped with a septum, and the mixture was let to homogenize during 1 h. Next, the flask was placed into an ice-bath for 10 min under moderate stirring. After this time, the cooled flask was uncapped, a sonication tip was introduced, and the solution was ultrasonicated for 3 min (Branson 250 Sonifier, analog cell disruptor 200 W max. output power; duty cycle 70%, output power control set at position 1). Once sonicated, the septum-capped flask was stirred for 10 min at RT, after which it was purged with N₂ for 10 min. Then, the flask was immersed in an oil bath (previously heated to 70 °C), and the polymerization was started after 4 min by adding 225 μL of KPS initiator (7.5 mg mL⁻¹). The mixture was gently stirred at 70 °C for 2 h, when the flask was removed from the oil bath and cooled down to RT. The product was split into five Eppendorf tubes and centrifuged at 21 000 × g for 10 min. The supernatants were discarded, the pellets redispersed in 200 μL of SDS (40 mM), diluted by adding 1 mL of deionized water (DI-H₂O), homogenized by vortexing, and centrifuged again. This cleaning process was repeated once again. As a final wash, the pellets were redispersed in 1.2 mL of DI-H₂O, centrifuged again, and redispersed and stored together into a final volume of 1 mL (DI-H₂O). The synthesis of UCNPs with a HPS composition of 75/25 vol% St/MMA, and with a composition of 50/50 vol% St/MMA, was performed similarly, but using 450 μL of St + 150 μL of MMA, and 450 μL of St and 450 μL of MMA, respectively. The parameters for all synthesis used in this work can be found in the Table S1, Supporting Information.

Synthesis of UCNPs-PAA (Standard Surface Functionalization; Control): Coating of oleate-capped UCNPs with a thin layer of PAA was performed as described elsewhere.^[72] 10 mg of UCNPs in hexane was split into two Eppendorf tubes and pelleted by centrifugation at 21 000 × g for 10 min. The resulting pellets were then gently dried, in order to remove the traces of hexane. Next, 1 mL of HCl (0.1 M) was added to each Eppendorf, and the pellets were redispersed by ultrasonication (5 min). The dispersed UCNPs were then incubated under vigorous shaking at RT for 5 h to remove the oleate molecules acting as capping agent, after which the UCNPs were recovered by centrifugation and the supernatant discarded. Then, the UCNPs were redispersed in 1 mL of DI-H₂O and centrifuged again. After discarding the supernatants, 1 mL of 2.5 wt% PAA aqueous solution (pH = 9) was added on top of each UCNPs pellet, which was dispersed by ultrasonication and vortexing. The reaction was incubated under vigorous shaking for 16 h at RT, allowing the formation of a thin PAA layer onto the UCNPs surface. UCNPs-PAA were recovered by centrifugation (21 000 × g, 10 min). Next, after discarding the

supernatants, the nanoparticles were dispersed in 1 mL of DI-H₂O, and this step was repeated twice. The resulting pellet was finally redispersed in 250 μL of DI-H₂O.

Long-Term Stability Assays at High Dilution and Room Temperature (DI-H₂O and Phosphate Buffer): Long-term stability studies of very diluted UCNPs samples (5 μg mL⁻¹ of UCNPs) were carried out in both DI-H₂O and 100 mM potassium phosphate buffer (K⁺PB). The authors analyzed the aging for the UCNPs with different polymer shells and their results were compared with UCNPs-PAA, used as a control sample. For each sample, as soon as it was diluted to 5 μg mL⁻¹ and transferred to the cuvette, it was placed inside the temperature controller cell holder (Jasco, ETC-273T), set at 25 °C. After 5 min (considered from here on as time zero), before any significant degradation occurred, the luminescence spectra were measured. Then, the luminescence spectra were measured several times during the next 72 h. For the analysis, all integrated luminescence intensities were normalized to the intensity obtained at time zero. Once the samples aged for 72 h, the authors also analyzed their decay time at RT and compared it with the decay times obtained for the corresponding not aged samples at a concentration of 100 μg mL⁻¹, when chemical degradation was negligible. For TEM characterization after the 72 h stability study in DI-H₂O, samples were concentrated by centrifuging at 21 000 × g during 30 min. In order to prepare the samples for HR-TEM characterization after the 72 h K⁺PB stability study, samples were centrifuged five times with DI-H₂O in order to remove excess buffer, and finally concentrated in DI-H₂O after the fifth centrifugation step.

Stability Assay at High Dilution and High Temperature (70 °C) in DI-H₂O: A long-term stability study of very diluted UCNPs-P75% samples in water at 5 μg mL⁻¹ was also carried out at high temperature (70 °C) to analyze the protective role of the HPS in comparison with that provided by the PAA layer. All spectra were taken at 25 °C to account only for the luminescence decrease due to degradation and not to thermometric properties of the UCNPs luminescence. The protocol was the following: right after diluting the samples at 5 μg mL⁻¹, the cuvette was introduced in the temperature controller cell holder at 25 °C, waited for sample temperature stabilization (5 min), and measured the time zero luminescence spectra. Then, temperature was increased up to 70 °C, waited for sample temperature stabilization (10 min), and left the samples at 70 °C for 1 h to permit the disintegration of the UCNPs. After 1 h at 70 °C, the temperature was decreased again to 25 °C, waited for sample temperature stabilization (20 min), and then measured the spectra again. The temperature cycle was repeated six more times up to 7 h. Once the experiments were finished, the authors also analyzed the luminescence decay time at RT of the samples and compared it with the decay times obtained for the corresponding not aged samples at a concentration of 100 μg mL⁻¹, when chemical degradation was negligible.

Supporting Information

Supporting Information is available from the Wiley Online Library or from the author.

Acknowledgements

This work has been funded by the Ministerio de Economía y Competitividad-MINECO (MAT2017-83111R), Ministerio de Ciencia, Innovación y Universidades-MICIU (RTI2018-094859-B-I00), Ministerio de Ciencia, Innovación y Universidades (PID2019-106211RB-I00; "NANONERV"), and by the Comunidad de Madrid (B2017/BMD-3867 RENIM-CM) cofinanced by European Structural and Investment Fund. D.M.-G. acknowledges UCM-Santander for a postdoctoral orientation period contract (CT17/17-CT18/17) and the Fundación para la investigación biomédica del Hospital Ramón y Cajal (FIBioHRyC), the Instituto Ramón y Cajal de Investigación Sanitaria (IRyCIS), and the European Commission Horizon 2020 project NanoTBTech (grant

number: 801305) for postdoctoral funding. I.Z.G. thanks UCM-Santander for a predoctoral contract (CT63/19-CT64/19). V.T.V. thanks Colfuturo and the Colombian government for a predoctoral scholarship. C.G. gratefully acknowledges the European Commission for the financial support through a Marie Skłodowska-Curie Action – Individual Fellowship (SPOT Action with Grant agreement ID 895932). The authors thank the staff at the ICTS-National Centre for Electron Microscopy (CNME) at the UCM and SCAI (UMA) for the help in the electron microscopy studies.

Conflict of Interest

The authors declare no conflict of interest.

Data Availability Statement

The data that support the findings of this study are available from the corresponding author upon reasonable request.

Keywords

degradation, dissolution, phosphates, polymers, protection, shells, upconversion nanoparticles

Received: September 15, 2021

Revised: November 4, 2021

Published online: December 13, 2021

- [1] S. Wu, G. Han, D. J. Milliron, S. Aloni, V. Altoe, D. v. Talapin, B. E. Cohen, P. J. Schuck, *Proc. Natl. Acad. Sci. USA* **2009**, *106*, 10917.
- [2] F. Wang, D. Banerjee, Y. Liu, X. Chen, X. Liu, *Analyst* **2010**, *135*, 1839.
- [3] G. Chen, H. Qiu, P. N. Prasad, X. Chen, *Chem. Rev.* **2014**, *114*, 5161.
- [4] W. R. Algar, M. Massey, K. Rees, R. Higgins, K. D. Krause, G. H. Darwish, W. J. Peveler, Z. Xiao, H.-Y. Tsai, R. Gupta, K. Lix, M. v. Tran, H. Kim, *Chem. Rev.* **2021**, *121*, 9243.
- [5] J. Zhou, Q. Liu, W. Feng, Y. Sun, F. Li, *Chem. Rev.* **2014**, *115*, 395.
- [6] D. Mendez-Gonzalez, S. Lahtinen, M. Laurenti, E. López-Cabarcos, J. Rubio-Retama, T. Soukka, *Anal. Chem.* **2018**, *90*, 13385.
- [7] E. Ortiz-Rivero, K. Prorok, M. Skowicki, D. Lu, A. Bednarkiewicz, D. Jaque, P. Haro-González, *Small* **2019**, *15*, 1904154.
- [8] F. Vetrone, R. Naccache, A. Zamarrón, A. J. de la Fuente, F. Sanz-Rodríguez, L. M. Maestro, E. M. Rodríguez, D. Jaque, J. G. Solé, J. A. Capobianco, *ACS Nano* **2010**, *4*, 3254.
- [9] Y. Xue, C. Ding, Y. Rong, Q. Ma, C. Pan, E. Wu, B. Wu, H. Zeng, *Small* **2017**, *13*, 1701155.
- [10] Z. Li, T. Liang, Q. Wang, Z. Liu, *Small* **2020**, *16*, 1905084.
- [11] Z. Zhang, Y. Zhang, *Small* **2021**, *17*, 2004552.
- [12] M. del Barrio, S. de Marcos, V. Cebolla, J. Heiland, S. Wilhelm, T. Hirsch, J. Galbán, *Biosens. Bioelectron.* **2014**, *59*, 14.
- [13] R. Arppe, I. Hyppänen, N. Perälä, R. Peltomaa, M. Kaiser, C. Würth, S. Christ, U. Resch-Genger, M. Schäferling, T. Soukka, *Nanoscale* **2015**, *7*, 11746.
- [14] S. Wilhelm, M. Kaiser, C. Würth, J. Heiland, C. Carrillo-Carrion, V. Muhr, O. S. Wolfbeis, W. J. Parak, U. Resch-Genger, T. Hirsch, *Nanoscale* **2015**, *7*, 1403.
- [15] S. Lahtinen, A. Lyytikäinen, H. Pääkilä, E. Hömppi, N. Perälä, M. Lastusaari, T. Soukka, *J. Phys. Chem. C* **2017**, *121*, 656.
- [16] O. Dukhno, F. Przybilla, V. Muhr, M. Buchner, T. Hirsch, Y. Mély, *Nanoscale* **2018**, *10*, 15904.
- [17] D. Lisjak, O. Plohl, M. Ponikvar-Svet, B. Majaron, *RSC Adv.* **2015**, *5*, 27393.

- [18] D. J. Gargas, E. M. Chan, A. D. Ostrowski, S. Aloni, M. V. P. Altoe, E. S. Barnard, B. Sani, J. J. Urban, D. J. Milliron, B. E. Cohen, P. J. Schuck, *Nanotechnol.* **2014**, *9*, 300.
- [19] I. Halimi, E. M. Rodrigues, S. L. Maurizio, H.-Q. T. Sun, M. Grewal, E. M. Boase, N. Liu, R. Marin, E. Hemmer, *J. Mater. Chem. C* **2019**, *7*, 15364.
- [20] G. Chen, T. Y. Ohulchanskyy, R. Kumar, H. Ågren, P. N. Prasad, *ACS Nano* **2010**, *4*, 3163.
- [21] B. Chen, W. Kong, N. Wang, G. Zhu, F. Wang, *Chem. Mater.* **2019**, *31*, 4779.
- [22] C. Würth, S. Fischer, B. Grauel, A. P. Alivisatos, U. Resch-Genger, *J. Am. Chem. Soc.* **2018**, *140*, 4922.
- [23] O. Plohl, M. Kraft, J. Kovac, B. Belec, M. Ponikvar-Svet, C. Würth, D. Lisjak, U. Resch-Genger, *Langmuir* **2017**, *33*, 553.
- [24] G. Zhao, L. Tong, P. Cao, M. Nitz, M. A. Winnik, *Langmuir* **2014**, *30*, 6980.
- [25] M. I. Saleh, B. Rühle, S. Wang, J. Radnik, Y. You, U. Resch-Genger, *Sci. Rep.* **2020**, *10*, 19318.
- [26] Y. C. Chang, M. Y. Chou, *Oral Surg., Oral Med., Oral Pathol., Oral Radiol.* **2001**, *91*, 230.
- [27] A. Verma, D. Ali, A. K. Pathak, *Toxicol. Environ. Chem.* **2017**, *99*, 148.
- [28] P. M. A. Salomão, F. A. de Oliveira, P. D. Rodrigues, L. P. Al-Ahij, K. C. da S. Gasque, P. Jeggle, M. A. R. Buzalaf, R. C. de Oliveira, J. M. Edwardson, A. C. Magalhães, *PLoS One* **2017**, *12*, e0179471.
- [29] S. Hirano, K. T. Suzuki, *Environ. Health Perspect.* **1996**, *104*, 85.
- [30] R. Li, Z. Ji, J. Dong, C. H. Chang, X. Wang, B. Sun, M. Wang, Y.-P. Liao, J. I. Zink, A. E. Nel, T. Xia, *ACS Nano* **2015**, *9*, 3293.
- [31] S. von Euw, Y. Wang, G. Laurent, C. Drouet, F. Babonneau, N. Nassif, T. Azaïs, *Sci. Rep.* **2019**, *9*, 8456.
- [32] E. Palo, M. Salomäki, M. Lastusaari, *J. Colloid Interface Sci.* **2019**, *538*, 320.
- [33] E. Palo, S. Lahtinen, H. Päckilä, M. Salomäki, T. Soukka, M. Lastusaari, *Langmuir* **2018**, *34*, 7759.
- [34] Q. Zhang, K. Song, J. Zhao, X. Kong, Y. Sun, X. Liu, Y. Zhang, Q. Zeng, H. Zhang, *J. Colloid Interface Sci.* **2009**, *336*, 171.
- [35] J.-C. Boyer, M.-P. Manseau, J. I. Murray, F. C. J. M. van Veggel, *Langmuir* **2009**, *26*, 1157.
- [36] S. F. Himmelstoß, T. Hirsch, *Part. Part. Syst. Character.* **2019**, *36*, 1900235.
- [37] U. Kostiv, V. Lobaz, J. Kučka, P. Švec, O. Sedláček, M. Hrubý, O. Janoušková, P. Francová, V. Kolářová, L. Šefc, D. Horák, *Nanoscale* **2017**, *9*, 16680.
- [38] P. Cao, L. Tong, Y. Hou, G. Zhao, G. Guerin, M. A. Winnik, M. Nitz, *Langmuir* **2012**, *28*, 12861.
- [39] G. Jiang, J. Pichaandi, N. J. J. Johnson, R. D. Burke, F. C. J. M. van Veggel, *Langmuir* **2012**, *28*, 3239.
- [40] M. Liras, M. González-Béjar, E. Peinado, L. Francés-Soriano, J. Pérez-Prieto, I. Quijada-Garrido, O. García, *Chem. Mater.* **2014**, *26*, 4014.
- [41] W. Zhang, B. Peng, F. Tian, W. Qin, X. Qian, *Anal. Chem.* **2014**, *86*, 482.
- [42] N. Estebanez, M. González-Béjar, J. Pérez-Prieto, *ACS Omega* **2019**, *4*, 3012.
- [43] Z. Li, Y. Zhang, *Nanotechnology* **2008**, *19*, 345606.
- [44] H. Chen, Y. Lang, D. Zhao, C. He, W. Qin, *J. Fluorine Chem.* **2015**, *174*, 70.
- [45] P. R. Griffiths, *Vib. Spectrosc.* **1992**, *4*, 121.
- [46] E. Andresen, C. Würth, C. Prinz, M. Michaelis, U. Resch-Genger, *Nanoscale* **2020**, *12*, 12589.
- [47] J. M. Asua, *Prog. Polym. Sci.* **2002**, *27*, 1283.
- [48] S. W. Zhang, S. X. Zhou, Y. M. Weng, L. M. Wu, *Langmuir* **2005**, *21*, 2124.
- [49] K. Landfester, in *Colloid Chemistry II* (Ed: M. Antonietti), Springer, Berlin **2003**, pp. 75–123.
- [50] G. Jia, Y. Xu, X. Tan, N. Cai, *Iran. Polym. J.* **2006**, *15*, 979.
- [51] S. Xu, W.-F. Ma, L.-J. You, J.-M. Li, J. Guo, J. J. Hu, C.-C. Wang, *Langmuir* **2012**, *28*, 3271.
- [52] J. Ge, Y. Hu, T. Zhang, Y. Yin, *J. Am. Chem. Soc.* **2007**, *129*, 8974.
- [53] C. Hübner, C. Fettkenhauer, K. Voges, D. C. Lupascu, *Langmuir* **2018**, *34*, 376.
- [54] Y. Li, B. Liu, *ACS Macro Lett.* **2017**, *6*, 1315.
- [55] C. S. Chern, C. H. Lin, *Polymer* **2000**, *41*, 4473.
- [56] M. Lundqvist, J. Stigler, G. Elia, I. Lynch, T. Cedervall, K. A. Dawson, *Proc. Natl. Acad. Sci. USA* **2008**, *105*, 14265.
- [57] J. A. Bonham, F. Waggett, M. A. Faers, J. S. van Duijneveldt, *Colloid Polym. Sci.* **2017**, *295*, 479.
- [58] J. Sefcik, M. Verduyn, G. Storti, M. Morbidelli, *Langmuir* **2003**, *19*, 4778.
- [59] A. Sedlmeier, H. H. Gorris, *Chem. Soc. Rev.* **2015**, *44*, 1526.
- [60] R. E. Farrell, in *RNA Methodologies*, Academic Press, Burlington **2005**, pp. 47–66.
- [61] Z. Zaman, R. L. Verwilghen, *Anal. Biochem.* **1979**, *100*, 64.
- [62] M. Vozlič, T. Černič, S. Gyergyek, B. Majaron, M. Ponikvar-Svet, U. Kostiv, D. Horák, D. Lisjak, *Dalton Trans.* **2021**, *50*, 6588.
- [63] R. Naccache, F. Vetrone, V. Mahalingam, L. A. Cuccia, J. A. Capobianco, *Chem. Mater.* **2009**, *21*, 717.
- [64] S. Märkl, A. Schroter, T. Hirsch, *Nano Lett.* **2020**, *20*, 8620.
- [65] E. Kang, H. Kim, L. A. G. Gray, D. Christie, U. Jonas, B. Graczykowski, E. M. Furst, R. D. Priestley, G. Fytas, *Macromolecules* **2018**, *21*, 8522.
- [66] T. S. Deng, J. H. Bongard, F. Marlow, *Mater. Chem. Phys.* **2015**, *162*, 548.
- [67] D. Sarma, P. Carl, E. Climent, R. J. Schneider, K. Rurack, *ACS Appl. Mater. Interfaces* **2019**, *11*, 1321.
- [68] R. A. Ramli, W. A. Laftah, S. Hashim, *RSC Adv.* **2013**, *36*, 15543.
- [69] Z. Zeng, J. Yu, Z. X. Guo, *Macromol. Chem. Phys.* **2004**, *16*, 2197.
- [70] A. Dong, X. Ye, J. Chen, Y. Kang, T. Gordon, J. M. Kikkawa, C. B. Murray, *J. Am. Chem. Soc.* **2011**, *133*, 998.
- [71] V. Muhr, C. Würth, M. Kraft, M. Buchner, A. J. Baeumner, U. Resch-Genger, T. Hirsch, *Anal. Chem.* **2017**, *89*, 4868.
- [72] N. Sirkka, A. Lyytikäinen, T. Savukoski, T. Soukka, *Anal. Chim. Acta* **2016**, *925*, 82.